Construction and Building Materials 425 (2024) 135976

Contents lists available at ScienceDirect

Construction and Building Materials

journal homepage: www.elsevier.com/locate/conbuildmat

Thermal stability and strength degradation of lithium slag geopolymer containing fly ash and silica fume

Usman Javed, Faiz Uddin Ahmed Shaikh *, Prabir Kumar Sarker

School of Civil and Mechanical Engineering, Curtin University, Perth, Australia

ARTICLE INFO

Keywords:
Thermal stability
microstructural evolution
surface porosity
crystal phase transformation
sintering
self-desiccation

ABSTRACT

This paper investigates the thermal stability of lithium slag geopolymer (LSG) containing fly ash (FA) and silica fume (SF) exposed up to 900℃. The effects of elevated temperatures on the microstructural evolution were investigated by thermogravimetric analysis (TGA), X-ray Diffraction (XRD), mineral analysis, surface porosity, and compressive strength of LSG modified by optimum incorporation of fly ash and silica fume. The results indicated that elevated temperature exposure significantly affects compressive strength, surface porosity, void size, weight loss, and phase transformation of fly ash incorporated lithium slag geopolymer (LSG_{FA}) and silica fume incorporated geopolymer (LSG_{SF}). The maximum loss in compressive strength of 44.07% was observed in LSG_{FA} compared to 31.50% loss in LSG_{SF} after exposure at 900℃. The weight loss of LSG_{SF} was higher than that of LSG_{FA} between 500 and 800℃ and 800–1000℃ indicating a higher degree of dehydroxylation, crystal phase transformation, and viscous sintering observed in the former mix. A larger shrinkage cracking was observed in LSG_{SF} by self-desiccation of the aluminosilicate paste matrix by dehydroxylation of mordenite molecules. Therefore, the degradation of compressive strength is governed by the combination of the crystallization of aluminosilicate gel and the formation of voids.

1. Introduction

The increasing focus on fire resistance of the building materials and safety measures has been driven by the frequent fire-related incidents in residential and public infrastructure. Every year, there are approximately 4 million reported fires globally, which lead to over 20,000 fatalities and 70,000 injuries. The majority of these fires originate in buildings and are frequently caused by the combustion of flammable materials [1].

Cement concrete exhibits impressive performance at room temperature, with production of about 25 billion tons in 2018 [2]; however, its structure is significantly weakened when exposed to elevated temperatures during fire event. A dense concrete microstructure that contains both water of hydration and physically attached water can potentially undergo explosive spalling when it is exposed to temperatures ranging from 300 to 450°C [3]. Additionally, once the temperature exceeds 400°C, the concrete will inevitably lose its ability to bear loads due to the decomposition of portlandite and this decomposition leads to irreversible structural changes [4].

Geopolymers, as a potential alternative to Portland cement, have shown better post-fire behavior. Recent studies [5–7] have demonstrated their superior fire resistance. The interest in fire-resistant materials originated from Davidovits' research after devastating fires caused by plastics in France during the early 1970 s [8]. Geopolymers have the impressive ability to maintain their strength even after being exposed to high temperatures. Additionally, they have significantly lower CO_2 emissions compared to ordinary Portland cement (OPC), which makes them a more environmentally friendly option [3].

Geopolymer binders are known for their anti-spalling properties synthesized by geopolymerization, which involves the formation of a strong three-dimensional aluminosilicate network framework. Geopolymers are beneficial for various applications such as fire-resistant coatings, thermal insulation, and wall panels due to their higher thermal stability [4]. Recent research has shown the increasing importance of geopolymers for passive fire protection in construction, specifically concerning the use of geopolymers for high-temperature applications [9–16]. However, even after conducting thorough investigations, there is still no agreement on mix designs or the factors that significantly affect

Abbreviations: LSG_{FA}, Lithium slag geopolymer containing fly ash; LSG_{SF}, Lithium slag geopolymer containing silica fume; TGA, Thermogravimetric analysis; XRD, X-ray Diffraction.

* Corresponding author.
E-mail address: s.ahmed@curtin.edu.au (F.U.A. Shaikh).

https://doi.org/10.1016/j.conbuildmat.2024.135976
Received 13 January 2024; Received in revised form 26 February 2024; Accepted 23 March 2024
Available online 1 April 2024

the fire performance of geopolymer. The published research suggests a lack of comprehensive understanding regarding the contributing factors for explaining the behaviour of geopolymers at elevated temperatures. The lack of understanding about the trends of strength evolution after exposure to elevated temperature is due to the diverse nature of precursors, and their complex composition which behave differently at varying elevated temperatures [17–19]. Various published research investigated the strength degradation of geopolymer containing ground granulated blast furnace slag and fly ash geopolymer [20–22]. Faiz et al. [21] investigated the fire resistance of fly ash-based fibre reinforced thermal coating for pine timber. The results indicated that the 4 mm potassium based geopolymer coating presented the highest resistance marked by 67–79% reduction in char depth after exposure to 1100℃ for 10 minutes. Cheng and Chiu [22] reported that the increasing concentration of K_2O enhance the resistance toward thermal degradation upon exposure to elevated temperature. Chindaprasirt and Rattanasak [20] reported the fire resistance of high calcium fly ash geopolymer bricks containing sodium hydroxide and sodium silicate as alkaline activator. The results of outdoor fire exposure up to 400℃ indicated the increasing trends and densification in microstructure by formation of Al-O-Si bonds and increasing Si/Al ratios. Therefore, the investigation of thermal resistance after exposure to elevated temperatures is important for determining the strength properties of geopolymer after fire exposure.

Current research is the pioneering study to investigate the thermal stability of LSG containing fly ash and silica fume at various elevated temperatures. The optimum mixes of fly ash and silica fume incorporated LSG from the authors' previous research were adopted to investigate the thermal stability and develop an understanding of the strength degradation mechanism [23]. The thermal stability of LSG containing fly ash and silica fume was conducted by analyzing TGA, XRD, mineral analysis, microstructural analysis, and strength degradation. For investigating the compressive strength deterioration, the compressive test results were compared with microscopic forensic analysis of LSG geopolymer specimens.

2. Materials and Methods

The raw materials used in this research were lithium slag, silica fume, and fly ash. The lithium slag was calcined at 700°C and then cooled to room temperature. After that, it was ground in a ball mill for half an hour. Thermo-mechanical processing is effective in increasing the amorphous phase [24,25]. The flash set of the geopolymer paste has been avoided by adding sodium tetraborate. Table 1 shows the chemical compositions of lithium slag, silica fume, and fly ash. The alkaline activators used were sodium hydroxide and sodium silicate. The sodium hydroxide solution had a molarity of 10 M. The sodium silicate consisted of 14.70% Na_2O, 29.40% SiO_2, and 55.90% water. The powdered borax consists of 99% concentrated sodium tetraborate decahydrate.

2.1. Chemical and morphological characterization

Comprehensive microstructural analysis was conducted on lithium slag using various techniques which are reported in the authors' previous research [23–25]. The microstructural characterization includes SEM/EDS, TIMA, XRD, XRF, and Rietveld Quantitative refinement. The investigation involved determining the chemical composition, crystallographic structure, and mineral phases. Fluorite was used as an internal standard for refinement. The study ensured that sample preparation and analysis parameters remained consistent with previous research [25]. The SEM examination showed that the fly ash particles varied in size, ranging from nanosized particles up to 10 μm. The bright fly ash cenospheres represent the presence of higher iron content evident from EDS analysis. The lithium slag showed the presence of calcium-rich aluminosilicates in the form of micro and nano-sized angular particles. The XRD and Rietveld quantitative analysis revealed the presence of higher amorphous phase content rich in aluminosilicates estimating the reactivity of lithium slag as a precursor. Along with the presence of aluminosilicates, the prismatic particles contained calcium sulphate, which is a byproduct of spodumene ore processing. The lower atomic number of sodium tetraborate decahydrate resulted in the absence of a visible boron peak, however, the highly perforated morphology of borate particles suggests the dissolution in a highly alkaline environment. The densified silica fume shows spherical particles with a nano-silica particle layer on the surface of the larger particles which can readily initiate the reaction at higher alkalinity. Therefore, the aluminosilicate-rich lithium slag, fly ash, and silica-rich silica fume present a suitable composition to improve the geopolymerization in LSG.

2.2. Mix proportions

The lithium slag geopolymer mixes were adopted from optimum mixes of the authors' previous research for investigating the fire resistance properties [23]. The optimum formulations were 50% and 40% replacement of lithium slag by fly ash and silica fume, respectively as shown in Table 1 [23]. The concentration of sodium hydroxide was chosen as 10 M. The geopolymer mixes were tested with alkaline activator contents of 45%. To enhance the strength development of the geopolymer, a 3% solution of sodium tetraborate decahydrate was included in all mixtures to slow down the rapid hardening process [23,24].

2.3. Casting and curing

The geopolymer specimens were created by combining fly ash and silica fume through dry mixing in a Hobart mixer for 30 seconds at a speed of 116 revolutions per minute (rpm). The resulting mix was then poured into alkaline activators and stirred for an additional 2 minutes at a speed of 380 rpm. The LSG_{FA} mix was placed into cube moulds of $50\times50\times50$ mm^3, followed by curing at 70°C for 24 h. To prevent any loss of moisture and the occurrence of microcracks, the moulds were covered with a polythene sheet. After 24 of heat curing, the LSG_{FA} paste specimens were subsequently stored at a temperature of 25 ± 1°C and a relative humidity of 90% until the testing age. Unlike LSG_{FA}, LSG_{SF} specimens were wrapped in a polythene sheet and stored at a temperature of $25° \pm 1$°C until the testing age. Silica fume incorporated mixes were not heat cured which induces strength degradation at accelerated curing as reported in author's previous research [24]. Thereafter, the mortar cube specimens were tested for compressive strength and microstructural investigation.

2.4. Exposure to elevated temperature

The LSG specimens containing fly ash and silica fume were exposed to 300, 500, 700, and 900℃ in the furnace. The heating rate was adopted as 15℃/min till the above-stated temperature and maintained these temperature exposures separately for two hours. The specimens were gradually cooled to room temperature by natural convection.

Table 1
Mix proportions of LSG containing fly ash and silica fume [23].

Activator (%)	Geopolymer mixes	Lithium slag (kg/m^3)	Fly ash (kg/m^3)	Sodium hydroxide (kg/m^3)	Sodium silicate (kg/m^3)	Borax (3%)
45	$50LS50FA_{45}$	707.93	707.93	159.28	477.85	42.47
45	$60LS40SF_{45}$	849.52	566.34	159.28	477.85	42.47

2.5. Testing methods

2.5.1. Thermogravimetric analysis

The TGA analysis was conducted using a TA Instruments SDT Q600 device that can measure both thermal and mass changes simultaneously. A small amount of sample (about 20 mg) was placed in a platinum crucible and heated from room temperature to 1000°C at a rate of 10°C per minute. The sample was exposed to a nitrogen gas flow of 100 ml per minute to prevent oxidation. The temperature and mass readings were calibrated using pure metals with known melting points and alumina standards. The heat flow was calibrated using a sapphire standard with a known heat capacity. The cell constant was adjusted using the latent heat of zinc. The TGA analysis provided information on the thermal stability, decomposition, and mass loss of the sample.

2.5.2. Crystal phase identification

The crystal phases in LSG paste were analyzed by X-ray diffraction (XRD). This study was conducted using a Bruker D8 Advance Diffractometer that emitted Cu_Kα X-rays. The phase identification was performed using DIFFRAC EVA software. The specimens were ring-milled and were filled in an acrylic sample holder followed by acquiring diffraction data.

2.5.3. Mineral analysis

Automated mineral analysis was performed on geopolymer paste specimens to investigate the variation in mineral composition upon exposure to elevated temperature. The mineral composition of the aluminosilicate gel matrix was quantified using an automated scanning electron microscope with energy-dispersive X-ray spectroscopy, namely the TESCAN Integrated Mineral Analyser (TIMA). The samples after fire exposure at 900℃ were sliced into chips (5×15×15 mm) using a cutter

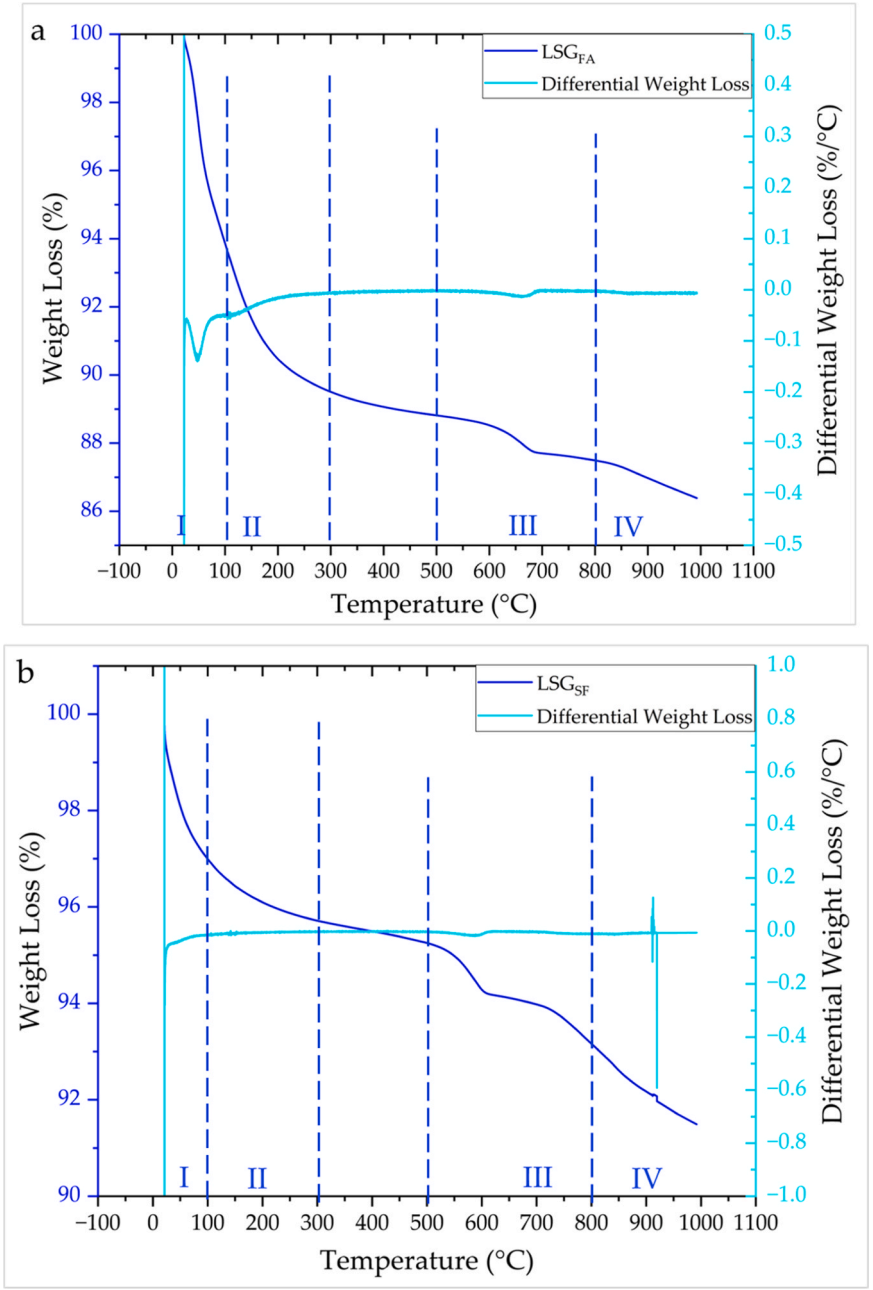

Fig. 1. The weight loss of LSG_{FA} and LSG_{SF} by thermogravimetric analysis.

with an adjustable speed up to 270 rpm. The vacuum-impregnated resin geopolymer specimens were analyzed using a high-resolution FESEM with four EDS detectors. The specimens were grinded to a roughness of 1 μm according to the standardized technique adopted in the literature [25]. The investigation was conducted using specific parameters, namely an electron beam energy of 25 keV, a probe current of 5.33 nA, and a beam intensity of 18.80.

2.5.4. Compressive strength

The compressive strength of geopolymer paste specimens was measured using a Shimadzu 300 kN universal testing machine. The specimens were tested before and after exposure to elevated temperature along with a constant loading rate of 0.24 MPa/s as per ASTM C109 standard [26].

3. Results and Analysis

3.1. Thermogravimetric analysis

The thermogravimetric analysis results of fly ash and silica fume incorporated LSG are shown in Fig. 1. The weight loss of LSG specimens is divided into four temperature zones are shown in Table 2. The temperature zones I, II, III, and IV are between temperatures of 21.28–100℃, 100–300℃, 500–800℃, and 800–1000℃, respectively. The weight loss of the geopolymer paste demonstrated the presence of aluminosilicate gel and the sintering temperatures of minerals in aluminosilicate gel. The weight loss in temperature zone-I is associated with the evaporation of pore water, followed by dehydroxylation (zone-II) between 100 and 300 C which involves the loss of bound water from the hydroxyl group of the geopolymer network which leads to reduced density and causes the mass loss. The rapid removal of chemically bound water by hydrogen bonding causes self-desiccation, attributing the pore formation [27]. During temperature zone-III, the combination of dehydroxylation of aluminosilicate gel occurs causing shrinkage of microstructure and transformation of mineral composition to new mineral phases which is also evident in literature [28,29]. In temperature zone IV, a continued viscous sintering process significantly diminishes porosity, induces thermal shrinkage, and further homogenizes and densifies the matrix [30,31], marked by the completion of the phase transformation.

The higher weight loss of the LSG_{FA} mix in the first two weight loss regions (zone-I & II) was observed with values of 6.13% and 4.29%, respectively which were higher than that of silica fume incorporated mixes. The higher weight loss in these regions corresponds with the higher degree of dissolution of aluminosilicate in fly ash incorporated LSG followed by the polycondensation processes which initiates the release of water. Upon the dissolution of aluminosilicate, water is utilized in the generation of different monomers, predominantly $SiO(OH)_2$, $Si(OH)_4$, and $Al(OH)_4$, as well as oligomers. Simultaneously, water is liberated as these monomeric and oligomeric species engage in polycondensation, initiating the polymerization and gelation of the solution [32,33]. After completion of the geopolymerization, water remained within the pores or firmly linked to the developed three-dimensional geopolymer network [32].

The weight loss of silica fume incorporated LSG is 2.08% and 1.67% in thermal regimes of 500–800℃ and 800–1000℃, respectively, which are higher than those of fly ash incorporated LSG at these temperature ranges. The higher weight loss of silica fume incorporated LSG is evident due to the higher degree of sintering of quartz at these temperatures. Although the sintering temperature of quartz is between 1200 and 1250℃, after treatment in highly alkaline (geopolymerization) and in the presence of borates the sintering of quartz appears to occur between 800 and 1000℃ [34]. Moreover, there is a considerable weight loss at 930℃ in silica fume incorporated LSG that might represent the complete melting of silica species in the geopolymer paste matrix. At elevated temperatures, the particles became soft and deformable and fused to form a denser and stronger structure by viscous sintering. Viscous sintering of geopolymer affected the microstructure by densification and pore refinement [35], altering the chemical composition of minerals disrupting the network of aluminosilicate, and inducing the formation of crystalline phases.

Similarly, Rickard et al. [30] reported the thermal properties of geopolymers made from fly ash with high iron and quartz content and revealed that the iron oxides affect the thermal expansion, phase composition, and morphology of the geopolymers after heating to 900°C. Another scientific aspect of sintering between 200°C to 1000°C reports the distinct chemical and crystal transformation in LSG_{SF} and LSG_{FA} geopolymers by the loss of chemically attached hydroxyl group and sintering, respectively. This phase transformation weakens the microstructure as new pores form alongside the recrystallization of the aluminosilicate gel. The aluminosilicate gel recrystallization could be affirmed by XRD analysis.

Table 2
Weight loss of LSG_{FA} and LSG_{SF} at various temperatures (*Mass loss is considered between 100 and 1000℃).

Temperature Range (C)	Temperature Zones	LSG_{SF}	LSG_{FA}
21.28–100	I	3.01	6.13
100–300	II	1.27	4.29
500–800	III	2.08	1.32
800–1000	IV	1.67	1.10
Total mass loss*		5.02	6.71

3.2. X-ray Diffraction

The major phases present in LSG_{FA} and LSG_{SF} were spodumene, albite, mordenite, anorthite, and calcite as investigated in authors' previous research [23,24]. The crystalline phases identified after exposure to elevated temperature were Quartz, Muscovite, Mullite, Aegirine Augite, Analcime, Calcite, Plagioclase, Anorthite, and Nepheline as shown in Fig. 2 & 3. The variation in crystallographic properties after thermal decomposition indicated that the feldspar phases underwent a transformation to aegirine-augite.

The XRD analysis of silica fume incorporated LSG showed that the spodumene peak disappeared after sintering the minerals at 900°C and a sharp Quartz peak emerged, whereas at 500°C the spodumene peak transformed into aegirine augite with low peaks of densified low-crystalline Quartz. There was also a noticeable crystallization of analcime, aegirine augite, and plagioclase at both temperatures, but with shifting peak positions upon calcination at higher temperatures. The

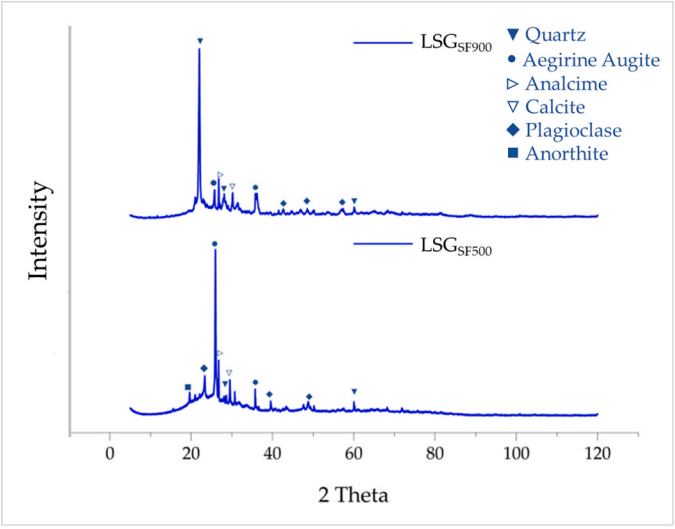

Fig. 2. XRD phase identification of LSG_{SF} at 500 and 900℃.

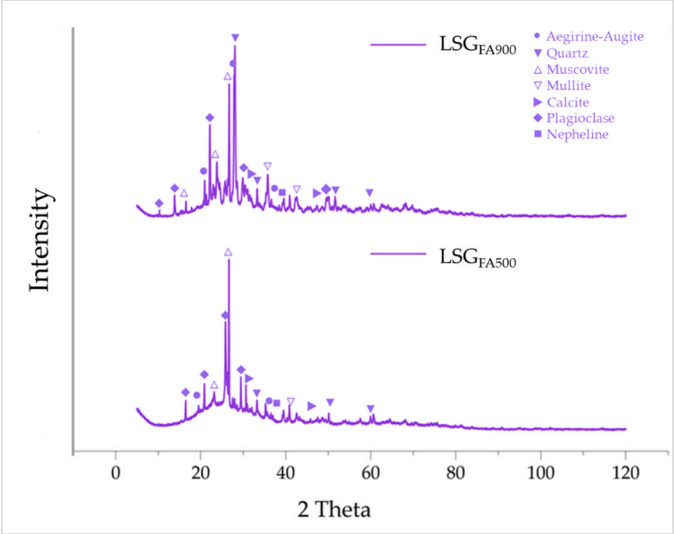

Fig. 3. XRD phase identification of LSG$_{FA}$ at 500 and 900℃.

peak shifts occurred due to changes in lattice parameters, crystal structure, and phase composition as reported in the literature [36]. The microstructure densification is carried out at higher sintering temperatures because of the viscous sintering of minerals. At elevated temperatures, the particles became soft and deformable and fused together to form a denser and stronger structure by viscous sintering. Viscous sintering of geopolymer affected the microstructure by densification and pore refinement [35], altering the chemical composition of minerals disrupting the network of aluminosilicate, and inducing the formation of crystalline phases.

The diffraction peaks at 500°C and 900°C indicated the formation of crystal phases after sintering. For both LSG$_{FA}$ and LSG$_{SF}$, the peak widening was observed at 900°C, indicating distortion of the lattice planes, phase transformation, and thermal expansion of the microstructure that changed interplanar distances [37,38]. In LSG$_{SF}$, aegirine augite and analcime crystallized at 500°C, whereas quartz, aegirine-augite, and analcime showed intense peaks at 900°C. In LSG$_{FA}$, muscovite and plagioclase had prominent peaks at 500°C, whereas quartz, muscovite, mullite, and aegirine augite were intensified at 900°C. Nepheline formation was evident in both fly ash and silica fume-incorporated geopolymer, which is consistent with the TIMA results. The crystal transformations upon exposure to elevated temperature caused variations in refractory properties and mechanical strength of geopolymer [39].

The minerals such as aegirine-augite, quartz, and analcime have higher sintering temperatures. However, the sintering temperature could be lowered by various factors such as higher alkaline content and Si/Al ratios [40]. Therefore, the sintering of the minerals may contribute to the densification of the microstructure, in addition to the dehydroxylation of the aluminosilicate gel matrix. Therefore, the crystal phase transformation is evident at both 500 and 900℃ which have impacts on the strength of the geopolymer.

3.3. Mineral analysis

The mineral composition of LSG containing fly ash and silica fume after exposure to elevated temperature (900℃) has been presented in Fig. 4a, and b, respectively. The mineralogy of LSG has been investigated in extensive detail in authors' previous studies which benchmark the mineral composition before exposure to elevated temperature [23,25]. Before exposure to the elevated temperature the aluminosilicate matrix of LSG containing fly ash was composed of 49.18, 29.32% of anorthite and mordenite, whereas anorthite and mordenite in silica fume

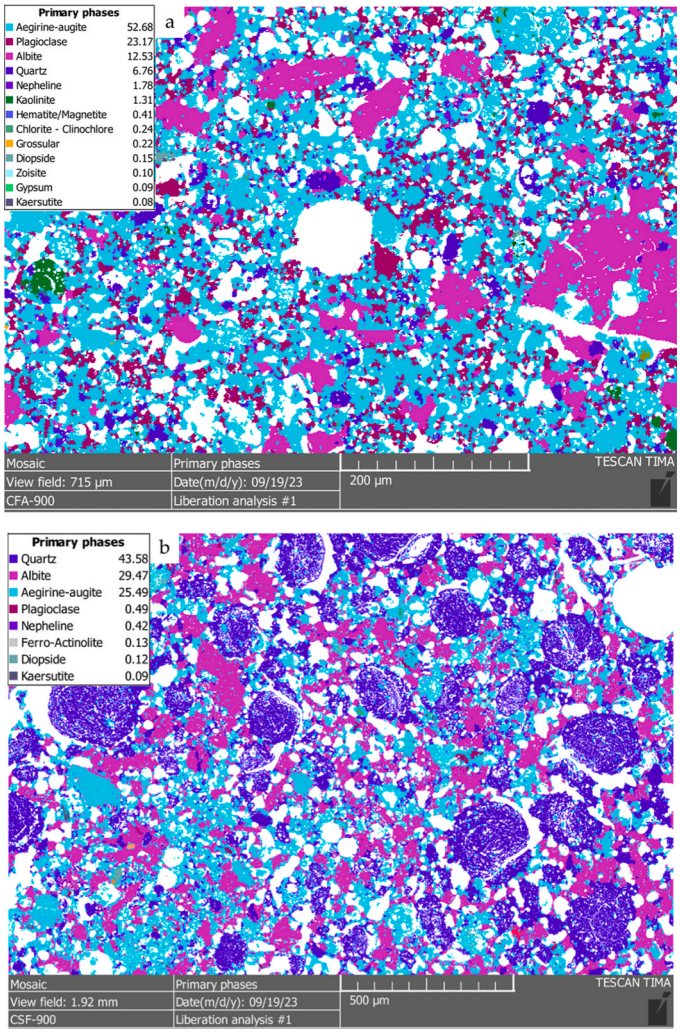

Fig. 4. Mineral composition of a: LSG$_{FA}$, b: LSG$_{SF}$ after exposure to elevated temperature (900℃).

incorporated LSG was 10.28%, and 29.21%, respectively.

After the sintering of LSG at higher temperatures the formation of product composition similar to aegirine-augite and plagioclase emerged possibly after the transformation of mordenite and anorthite, respectively. The fly ash LSG is composed of aegirine-augite and plagioclase as a sintered binding phase, whereas the aegirine-augite and albite are the dominating sintering phases in silica fume LSG. Nepheline formed in the silica fume and fly ash incorporated LSG is observed as 1.78% and 0.49%, respectively which contribute toward the densification upon sintering as evident from the literature [41]. Aegirine-augite, plagioclase, and albite are the contributing mineral phases toward the strength development of both silica fume and fly ash incorporated LSG. The transformation of crystal phases with the effect of high temperature is evident from the XRD analysis which is consistent with the mineral analysis results. Similarly, Stoch et al. [42] revealed the formation of aegirine-augite and wollastonite as a crystal phase after sintering of hospital incinerated ash with borosilicate glass between 800 and 900℃. The aegirine-augite, nepheline, has higher thermal stability and chemical resistance than the mordenite phase formed in geopolymer. However, the induced porosity during sintering has effects on the compressive strength of the geopolymer which is discussed in a subsequent section.

3.4. Effect of sintering on porosity

Exposure of fly ash and silica fume incorporated LSG to elevated temperature resulted in the formation of porosity in the microstructure, as shown in Fig. 5. The SEM micrographs of the LSG geopolymer contain the colored filter for depicting the intensity of BSE. Alongside the thermal decomposition of gel matrix and mineral particles, the phase transformation and fluxing of minerals to form complexes were also revealed in the micrograph. The bright regions represent the Fe-containing mineral in fly ash particles, whereas the dark regions represent the pores and voids, whereas the bright microstructure on silica particles after exposure to elevated temperature shows the formation of aegirine-augite particles, as evident from mineral micrographs (Fig. 5).

The percentage voids in LSG_{FA} and LSG_{SF} specimens were 23.73% and 26.863%, respectively. The LSG_{SF} specimen showed larger voids than the LSG_{FA} specimen. The voids are classified into two types i.e. macro and micro pores. The smallest set of pores observed was 1 micron and smaller pores cannot be captured because of the limitation of the smallest pixel size of 1 μm, however, the maximum size of the pore for LSG_{FA} and LSG_{SF} specimens are 60 and 120 μm, respectively. The sintering of the LSG specimens results in dehydration, dehydroxylation, phase recrystallization, weight loss, relative shrinkage, and expansion in the geopolymer paste matrix which is discussed in thermogravimetric analysis. The decomposition and recrystallization of aluminosilicate gel, differing fusion temperatures, and expansion coefficients of the minerals caused the microstructural deterioration.

Similarly, the published literature has reported the effects of sintering on the geopolymer paste matrix [43,44]. Ye et al. (2014) investigated the effect of exposure to elevated temperatures on the properties of geopolymer synthesized from calcined ore-dressing tailing of bauxite and ground-granulated blast furnace slag. The results indicated that the geopolymer mortars experience cracking, shrinkage, expansion, strength loss, and gain after heating from ambient temperature to 1200°C. Liu et al. (2020) investigated the effects of incorporating rice husk ash in a metakaolin-based geopolymer, the results indicated that the optimum rice husk ash content was 15% metakaolin, which enhanced the compressive strength by 24% and lowered the sintering temperature by 90°C. Therefore, the deterioration of the microstructure is governed by the chemical crystallization of aluminosilicate gel and the formation of pores and voids.

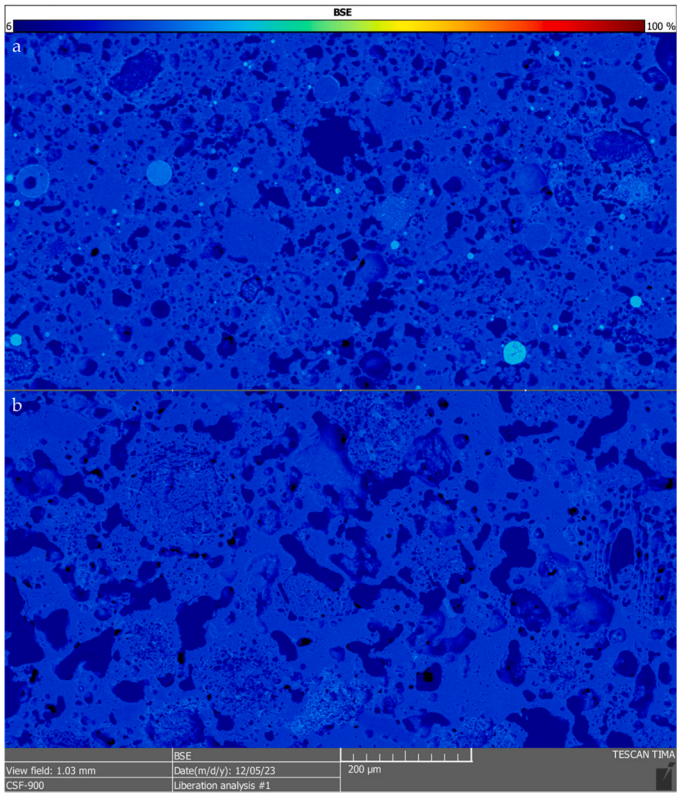

Fig. 5. Comparison of porosity and relative sintering of the LSG after exposure to elevated temperature (900C) a) LSG_{FA} b) LSG_{SF}.

3.5. Compressive strength

The compressive strength of fly ash and silica fume incorporated LSG exposed to elevated temperatures is shown in Fig. 6. There is a general trend of drop in compressive strength observed for both silica fume and fly ash incorporated LSG. The drop in compressive strength from 48.22 MPa to 39.10, 30.74, 28.89, and 33.03 MPa was recorded at 300, 500, 700, and 900℃, respectively for the LSG_{SF} mix. The decrease in compressive strength for the LSG_{FA} mix was from 42.68 MPa to 36.51, 31.14, 25.38, and 23.87 MPa, respectively.

The percentage loss of the LSG containing silica fume and fly ash was 18.91, 36.25, 40.08, 31.50%, and 14.45, 27.03, 40.53, 44.07%, respectively. At lower temperatures, the strength degradation of fly ash incorporated LSG was lower than that of silica fume incorporated LSG, whereas silica fume specimens experienced less strength degradation at 900℃, possibly due to the viscous sintering of silicon dioxide in silica fume particles. Similarly, Ye et al. [43] explored the effect of elevated temperatures on the geopolymer produced by calcined bauxite ore-dressing tailings and ground-granulated blast furnace slag. The compressive strength of the mortar initially declined with rising temperatures up to 1000°C, attributed to gel cracking, decomposition, and crystallization.

4. Discussion

4.1. Thermal decomposition of microstructure

LSG pastes' performance at elevated temperatures depends significantly on gel formation, pore structure, and phase transitions within its components. The microstructure of LSG_{FA} and LSG_{SF} after sintering was observed from BSE images, which showed the presence of surface pores that corresponded to the weight loss regions determined by thermogravimetric analysis. These pores are generated by aluminosilicate gel

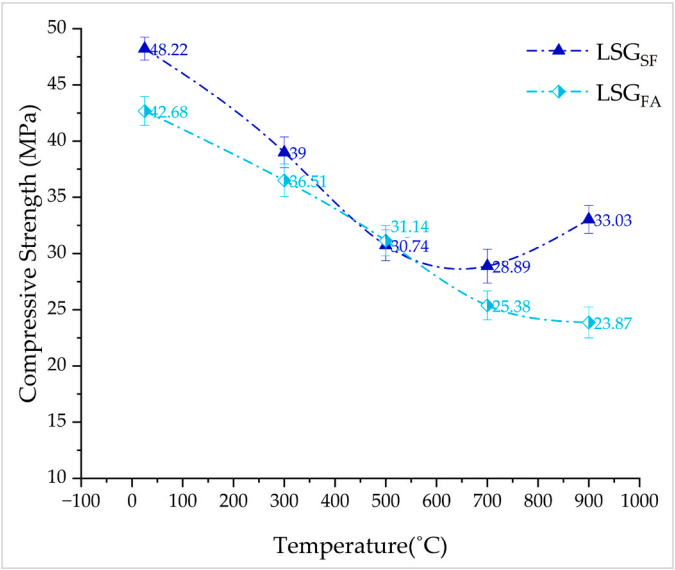

Fig. 6. The strength loss upon exposure to higher temperatures.

matrix shrinkage, leading to a denser microstructure owing to dehydration and dehydroxylation at elevated temperatures. Microstructural modifications, such as changes in pore sizes and composition, are induced by dehydration, dehydroxylation, and phase changes that occur during sintering. The pore size in silica fume-incorporated LSG was larger than that of fly ash-incorporated geopolymer paste matrix. Larger pore sizes (10–50 microns) in LSG_{SF} specimens were attributed to dehydroxylation and phase transformation of mordenite species between 500 and 800°C (XRD). Weight loss of LSG_{SF} and LSG_{FA} between 500 and 800°C was recorded as 2.08% and 1.32%, respectively. The higher-density anorthite phase in LSG_{FA} offered greater resistance to thermal decomposition compared to lower-density mordenite phase in LSG_{SF}. The temperature regime between 800 and 1000°C was associated with thermal decomposition and crystallographic transformation of minerals such as quartz, albite, and spodumene, resulting in micro and nano-sized pores. The higher number of pores in silica particles of the LSG_{SF} mix indicated higher sintering around 930°C, marked by the onset of fusion of silica particles. The fusion of silica flux altered microstructure, inducing more stiffness but also resulting in negative impacts of thermal decomposition of aluminosilicate gel between 500 and 800°C, and shrinkage cracking. Aluminosilicate particles, such as spodumene and albite, exhibited greater resistance to fusion but underwent significant thermal decomposition. Due to viscous sintering, a drastic drop in compressive strength was not observed [45]. The strength loss from dehydroxylation might have been compensated by strength gain from microstructure densification.

4.2. Influence on aluminosilicate gel matrix

Aluminosilicate gel microstructure dictates pore morphology, directly influencing water transport and spalling resistance in geopolymers. During heating, water evaporates from gel pores leaving voids. If pores are connected, water escapes without causing spalling; otherwise, the stress in pore walls during water escape can lead to collapse and shrinkage cracking. The specimens exhibited no spalling under high-temperature conditions, indicating the presence of interconnected micro-pores. The Si-O-Al network formed during gelation predominantly creates a mesoporous structure, filling large pores [46]. The higher shrinkage cracking has been observed in LSG_{SF} by self-desiccation of aluminosilicate paste matrix owing to the higher physically attached water content in mordenite molecules. At elevated temperatures, LSG specimens experienced dehydration, dehydroxylation, and phase recrystallization of the geopolymer paste matrix [43, 44].

4.3. Phase transitioning

Alkali feldspars (albite, anorthite) within geopolymers exhibit distinct chemical compositions and thermal behaviour [46]. The phases present in LSG_{FA} and LSG_{SF} were spodumene, albite, mordenite, and anorthite [23,24]. The feldspar phases underwent a transformation to aegirine-augite upon exposure to elevated temperature. The crystallization temperature of these phases varies based on alkali content and precursor composition [47]. Upon heating, geopolymers generate a non-equilibrium melt, leading to the creation of new crystalline phases. SiO_2 diffusion into the reaction zone escalates with temperature, engaging primarily in the breakdown of unstable crystalline structures and sintering of the SiO_2-Al_2O_3 matrix, incorporating alkali ions from raw materials and the activator solution. Feldspar phases remain stable until reaching their melting point, with thermo-stable nepheline plagioclase phases formed between 800 and 1000°C enhancing thermal stability [48]. The sintering of LSG at elevated temperatures led to the formation of aegirine-augite and plagioclase, mainly from mordenite and anorthite transformations. Notably, fly ash LSG mainly comprised of aegirine-augite and plagioclase as sintered binding phases, while silica fume LSG depicted aegirine-augite and albite as dominant sintering phases. The presence of nepheline in both types of LSG contributed to densification upon sintering. Therefore, the phase transitioning and phase crystallization has resulted notable improvements in strength development of LSG_{SF} at 900℃.

5. Conclusions

The article investigates for the first time the exposure of LSG containing fly ash and silica fume to elevated temperatures. The results of surface porosity, mineral analysis, and TGA unrevealed interesting insights about the thermal stability and minerals formation in LSG_{FA} and LSG_{SF} at various elevated temperature up to 900℃. The dehydroxylation, crystal phase transformation, thermal cracking, and evolution of pore structure are the dominant causes of the variation in compressive strength. The following are the salient conclusions drawn from the study:

1. The sintering of LSG induces phase transformations, pore formation, and strength loss upon incorporation of both fly ash and silica fume, but the extent and nature of these changes depend on the Si/Al ratio, and mineralogy of aluminosilicate gel. Therefore, the sintering of LSG results in physical, crystallographic and chemical changes in its microstructure.
2. LSG_{FA} has higher thermal stability and resistance to dehydroxylation than LSG_{SF} up to 300℃, but silica fume incorporated LSG exhibits less shrinkage cracking and higher residual strength at 900°C due to the viscous sintering of silica-fume particles. Hence, LSG_{SF} specimens are suitable to resistance of thermal deterioration and ensure more thermal stability at 900℃.
3. The overall strength loss of LSG_{FA} was lower than that of LSG_{SF} at 300℃, however, the lower strength loss was observed for LSG_{SF} at 900℃. However, the strength degradation was 31.50% and 44.07% for LSG_{SF}, LSG_{FA} at 900℃. The lower strength degradation of LSG_{SF} at higher temperature increased the fire resistance and subsequently enhanced structural adequacy of LSG upon silica fume incorporation.
4. The sintering of LSG at elevated temperatures led to the formation of aegirine-augite and plagioclase, mainly from mordenite and anorthite transformations. The LSG_{FA} mainly comprised aegirine-augite and plagioclase as sintered binding phases, while LSG_{SF} depicted aegirine-augite and albite as dominant sintering phases.
5. The formation of ceramic product (nepheline) in both types of LSG may have contributed to densification upon sintering. The strength loss of LSG was attributed to dehydration, dehydroxylation, and phase changes that occurred during sintering. Viscous sintering of LSG_{SF} is evidenced marked by higher weight loss in TGA which enhanced the microstructure by densification and pore refinement at 900℃.

CRediT authorship contribution statement

Usman Javed: Writing – original draft, Methodology, Investigation, Formal analysis, Conceptualization, Visualization. **Faiz Uddin Ahmed Shaikh:** Writing – review & editing, Supervision, Resources, Funding acquisition, Conceptualization. **Prabir Kumar Sarker:** Writing – review & editing, Supervision.

Declaration of Competing Interest

The authors declare that they have no known competing financial interests or personal relationships that could have appeared to influence the work reported in this paper.

Data Availability

Data will be made available on request.

Acknowledgment

The authors acknowledge to Australian Research Council (ARC), Australia for providing financial support in this research in the form of Discovery Project grant DP200102784.

The authors also acknowledge the use of the state-of-the-art Tescan Integrated Mineral Analyzer (TIMA), and X-ray Diffractometer (D8 Discover) at John De Laeter Centre, Curtin University, Australia.

References

[1] CTIF, CTIF World Fire Statistics Report No 27, 2023. https://ctif.org/news/ctif-world-fire-statistics-report-no-27-now-available-download. (Accessed 02.12.2023 2023).
[2] G.V. Research, Fire protection Materials Market for Construction Inudstry Analysis Report, 2015. https://www.grandviewresearch.com/industry-analysis/fire-protection-materials-market/methodology. 2023).
[3] K.D. Hertz, Limits of spalling of fire-exposed concrete, Fire Saf. J. 38 (2) (2003) 103–116.
[4] L. Alarcon-Ruiz, G. Platret, E. Massieu, A. Ehrlacher, The use of thermal analysis in assessing the effect of temperature on a cement paste, Cem. Concr. Res. 35 (3) (2005) 609–613.
[5] P. Duxson, G.C. Lukey, J.S.J. van Deventer, Thermal conductivity of metakaolin geopolymers used as a first approximation for determining gel interconnectivity, Ind. Eng. Chem. Res. 45 (23) (2006) 7781–7788.
[6] W.D.A. Rickard, C.D. Borstel, A. van Riessen, The effect of pre-treatment on the thermal performance of fly ash geopolymers, Thermochim. Acta 573 (2013) 130–137.
[7] W.D.A. Rickard, G.J.G. Gluth, K. Pistol, In-situ thermo-mechanical testing of fly ash geopolymer concretes made with quartz and expanded clay aggregates, Cem. Concr. Res. 80 (2016) 33–43.
[8] J. Davidovits, years of successes and failures in geopolymer applications. Market trends and potential breakthroughs, Geopolymer 2002 conference, Geopolymer Institute Saint-Quentin, France; Melbourne, Australia, 2002, p. 29.
[9] V. Le, P. Louda, Research of Curing Time and Temperature-Dependent Strengths and Fire Resistance of Geopolymer Foam Coated on an Aluminum Plate, Coatings 11 (1) (2021).
[10] M. Ozawa, F.U.A. Shaikh, A study on spalling behaviour of geopolymer mortars using ring restraint test, Constr. Build. Mater. 279 (2021).
[11] I. Hager, M. Sitarz, K. Mróz, Fly-ash based geopolymer mortar for high-temperature application - Effect of slag addition, J. Clean. Prod. 316 (2021).
[12] J.C. Kuri, S. Majhi, P.K. Sarker, A. Mukherjee, Microstructural and non-destructive investigation of the effect of high temperature exposure on ground ferronickel slag blended fly ash geopolymer mortars, J. Build. Eng. 43 (2021).
[13] M. Sivasakthi, R. Jeyalakshmi, N. Rajamane, Fly ash geopolymer mortar: Impact of the substitution of river sand by copper slag as a fine aggregate on its thermal resistance properties, J. Clean. Prod. 279 (2021) 123766.
[14] K. Traven, M. Cesnovar, S.D. Skapin, V. Ducman, High temperature resistant fly-ash and metakaolin-based alkali-activated foams, Ceram. Int. 47 (17) (2021) 25105–25120.
[15] O.H. Li, L. Yun-Ming, H. Cheng-Yong, R. Bayuaji, M.M.A. Abdullah, F.K. Loong, T. S. Jin, N.H. Teng, M. Nabialek, B. Jez, N.Y. Sing, Evaluation of the Effect of Silica Fume on Amorphous Fly Ash Geopolymers Exposed to Elevated Temperature, Magnetochemistry 7 (1) (2021).
[16] M.E. Kalaw, J.M. Adiarte, R. dela Cruz, K.M. Martinez, C.A. Vega, M. A. Promentilla, Strength and fire resistance characteristics of geopolymers synthesized from volcanic ash, red clay and waste pen shells. IOP Conference Series: Materials Science and Engineering, IOP Publishing, 2021 012068.
[17] M.K. Lahoti, K.H. Tan, E.H. Yang, A critical review of geopolymer properties for structural fire-resistance applications, Constr. Build. Mater. 221 (2019) 514–526.
[18] A. Hassan, M. Arif, M. Shariq, T. Alomayri, S. Pereira, Fire resistance characteristics of geopolymer concrete for environmental sustainability: a review of thermal, Mech. Microstruct. Prop., Environ. Dev. Sustain 25 (9) (2023) 8975–9010.
[19] S. Luhar, D. Nicolaides, I. Luhar, Fire resistance behaviour of geopolymer concrete: an overview, Buildings 11 (3) (2021).
[20] P. Chindaprasirt, U. Rattanasak, Fire-resistant geopolymer bricks synthesized from high-calcium fly ash with outdoor heat exposure, Clean. Technol. Environ. 20 (5) (2018) 1097–1103.
[21] U.A.S. Faiz, Haque Sharany, Sanjayan Jay, Behavior of fly ash geopolymer as fire resistant coating for timber, J. Sustain. Cem. -Based Mater. 8 (5) (2019) 259–274.
[22] T.W. Cheng, J.P. Chiu, Fire-resistant geopolymer produced by granulated blast furnace slag, Miner. Eng. 16 (3) (2003) 205–210.
[23] U. Javed, F.U.A. Shaikh, P.K. Sarker, A comprehensive micro-nano investigative approach to study the development of aluminosilicate gel in binary blends of lithium slag geopolymer, Cem. Concr. Comp. 145 (2024).
[24] U. Javed, F.U.A. Shaikh, P.K. Sarker, Microstructural investigation of lithium slag geopolymer pastes containing silica fume and fly ash as additive chemical modifiers, Cem. Concr. Comp. 134 (2022).
[25] U. Javed, F.U.A. Shaikh, P.K. Sarker, Microstructural investigation of thermo-mechanically processed lithium slag for geopolymer precursor using various characterization techniques, Constr. Build. Mater. 342 (2022).
[26] ASTM, Standard test method for compressive strength of hydraulic cement mortars (using 2-in. or [50-mm] cube specimens), Annual Book of ASTM StandardsAnnual Book of ASTM Standards 4(1) (2013) 1–9.
[27] Y. Zhang, J.L. Zhang, J.Y. Jiang, D.S. Hou, J.R. Zhang, The effect of water molecules on the structure, dynamics, and mechanical properties of sodium aluminosilicate hydrate (NASH) gel: a molecular dynamics study, Constr. Build. Mater. 193 (2018) 491–500.
[28] W.D.A. Rickard, A. van Riessen, P. Walls, Thermal character of geopolymers synthesized from class F fly ash containing high concentrations of iron and α-quartz, Int J. Appl. Ceram. Tec. 7 (1) (2010) 81–88.
[29] P. Duxson, G.C. Lukey, J.S.J. van Deventer, Physical evolution of Na-geopolymer derived from metakaolin up to 1000°C, J. Mater. Sci. 42 (9) (2007) 3044–3054.
[30] W. Rickard, Temuujin Van Riessen, Thermal analysis of geopolymer pastes synthesised from five fly ashes of variable composition, J. Non-Cryst. Solids 358 (15) (2012) 1830–1839.
[31] F.U.A. Shaikh, V. Vimonsatit, Compressive strength of fly-ash-based geopolymer concrete at elevated temperatures, Fire Mater. 39 (2) (2015) 174–188.
[32] J. Davidovits, Geopolymer, Chemistry and Applications. Institute Geopolymere, Saint-Quentin, France (2008).
[33] D. Perera, O. Uchida, E. Vance, K. Finnie, Influence of curing schedule on the integrity of geopolymers, J. Mater. Sci. 42 (2007) 3099–3106.
[34] L. Zeng, H.J. Sun, T.J. Peng, Effect of borax on sintering kinetics, microstructure and mechanical properties of porous glass-ceramics from coal fly ash by direct overfiring, Front. Chem. 10 (2022).
[35] A. Nana, G. Ridolfi, C.S.D. Anensong, S.B.L. Ngomade, A.A. Adediran, J. Ngouné, E. Kamseu, M.C. Bignozzi, C. Leonelli, Thermal, mechanical, and microstructural properties of inorganic polymer composites from quarry wastes (feldspathic minerals), J. Therm. Anal. Calorim. 148 (19) (2023) 10021–10035.
[36] Y.X. Li, X.L. Wang, L.M. Ding, Y. Li, R.C. He, J. Li, Changing the calcination temperature to tune the microstructure and polishing properties of ceria octahedrons, RSC Adv. 12 (26) (2022) 16554–16560.
[37] P. Singh, V. Shrivastava, I.B. Singh, D.P. Mondal, Effect of mechanical alloying and sintering environment on the crystallographic evolution, microstructure, mechanical and corrosion properties of porous Ti4Al4Co alloy, Met. Mater. Int. 28 (6) (2022) 1455–1470.
[38] Z.Q. Shi, Q.L. Zhao, B. Guo, T.Y. Ji, H. Wang, A review on processing polycrystalline magnesium aluminate spinel (MgAlO): sintering techniques, material properties and machinability, Mater. Des. (193 () (2020).
[39] E. Kamseu, C. Djangang, P. Veronesi, A. Fernanda, U.C. Melo, V.M. Sglavo, C. Leonelli, Transformation of the geopolymer gels to crystalline bonds in cold-setting refractory concretes: pore evolution, mechanical strength and microstructure, Mater. Des. 88 (2015) 336–344.
[40] H.W. Hu, K. Zhou, K.S. Meng, L.B. Song, Q.Z. Lin, Effects of SiO/AlO ratios on sintering characteristics of synthetic coal ash, Energies 10 (2) (2017).
[41] N.B. Mustapa, R. Ahmad, M.M.A.B. Abdullah, W.M.W. Ibrahim, A.V. Sandu, C. W. Kartikowati, P. Risdanareni, W.H.W.M. Saimi, Densification Behavior and Mechanical Performance of Nepheline Geopolymer Ceramics: Preliminary Study. International Conference on Innovative Research, Springer, 2023, pp. 184–192.
[42] P. Stoch, M. Ciecinska, A. Stoch, L. Kuterasinski, I. Krakowiak, Immobilization of hospital waste incineration ashes in glass-ceramic composites, Ceram. Int. 44 (1) (2018) 728–734.
[43] J.Y. Ye, W.S. Zhang, D. Shi, Effect of elevated temperature on the properties of geopolymer synthesized from calcined ore-dressing tailing of bauxite and ground-granulated blast furnace slag, Constr. Build. Mater. 69 (2014) 41–48.
[44] X.H. Liu, J.P. Jiang, H.L. Zhang, M.S. Li, Y.Y. Wu, L. Guo, W.Q. Wang, P. Duan, W. S. Zhang, Z.H. Zhang, Thermal stability and microstructure of metakaolin-based geopolymer blended with rice husk ash, Appl. Clay Sci. 196 (2020).
[45] S. Yasin, H. Ahlatci, Thermal investigation of fine alumina powder reinforced Na-metakaolin-based geopolymer binder for refractory applications, J. Aust. Ceram. Soc. 55 (2) (2019) 587–593.
[46] J.Van Deventer Sindhunata, G. Lukey, H. Xu, Effect of curing temperature and silicate concentration on fly-ash-based geopolymerization, Ind. Eng. Chem. Res. 45 (10) (2006) 3559–3568.
[47] P. Ptácek, F. Soukal, T. Opravil, E. Bartonícková, J. Wasserbauer, The formation of feldspar strontian (SrAlSiO) via ceramic route: reaction mechanism, kinetics and thermodynamics of the process, Ceram. Int. 42 (7) (2016) 8170–8178.
[48] J.S.J.V.D.J.L. Provis, Geopolymers: structure, processing, properties and industrial applications, Woodhead Publ. Mater. (2009) 1–454.